RESEARCH ARTICLE

Macromolecular Bioscience
www.mbs-journal.de

Magnetically Active Bicontinuous Polymer Structures for Multiple Controlled Drug Delivery

*Elisa Lacroce, Fabio Pizzetti, Nicolás M. Barbosa Urrego, Giuseppe Nunziata, Maurizio Masi, and Filippo Rossi**

The targeted delivery of drugs using wireless navigable magnetic robots allows the delivery of drug molecules to be controlled non only in time but also in space, improving medical outcomes. The main disadvantages behind their use lies in the low amount of drug that can be transported and the single nature of drug that can be loaded (hydrophilic or hydrophobic). These considerations limit their use in co-delivery systems, now recognized to be very promising for many different pathologies. A magnetic bijel-like structure is developed to load and release different types of molecules (hydrophilic and hydrophobic). In this work, the use of ϵ-caprolactone is explored, which can polymerize, forming hydrophobic domains (oil phase). After mixing with iron oxide nanoparticles (NPs), the water dispersion creates a magnetic biphasic porous structure without phase separation. The resulting device shows good performance both in magnetic actuation and as a drug delivery system.

1. Introduction

Routes for drug administration and their relative pharmacokinetics inside the body are among the most critical issues in ultramodern medicine.[1,2] Indeed, the effectiveness of recently developed pharmaceutical agents is strictly limited by traditional administration strategies.[3,4] They are based on the non-selective distribution of the active ingredient throughout the body, intermediated by the bloodstream. The high clearance associated with blood circulation and the consequent inefficient administration of the active ingredient forces the use of higher amounts of the drug, increasing costs and drawbacks for the patient.[5,6] For this reason, recent advanced administration strategies are aimed at guaranteeing targeted delivery. Drug molecules can be released in controlled quantities accordingly and only in the target organ, avoiding distribution across the whole body and limiting the invasiveness of the therapy. Numerous varieties of smart delivery approaches have been described in the recent literature.[7,8] Many of them focus on nanostructures capable of traveling through the blood system until they reach the target organ where the pharmacological activity takes place. Such is the case with delivery systems that consider liposomes,[9] polymeric micelles,[10] nanoparticles,[11] microspheres, and DNA composite nanostructures.[12] However, despite many good results in preclinical studies, persisting doubts relate to toxicological aspects and reliable manufacturing procedures.[13,14] Other extremely promising approaches to advanced targeted drug delivery have recently been developed. One method focuses on controlled release devices using wirelessly navigable robots.[15–17] Small-scale robots can be guided toward the target organ inside the human body for localized drug delivery. Since they are designed for in vivo use, their locomotion strategy is a crucial aspect. Indeed, among the different remote actuation methods (light, chemical, or ultrasounds) that have been proposed, magnetic actuation seems to be the most promising.[18–20] A large number of functional micro- and nano-devices have been presented in the literature covering operational fields such as localized surgery, bacteria disinfection, cell delivery, and also drug delivery.[21–23] Targeted delivery using magnetic-driven microrobots can be done using different techniques based on metals or metal-coated devices.[24–26]

The presence of an organic external layer (coating) creates a drug reservoir for the controlled release of active molecules loaded in[27,28] or linked to the external layer.[21] One of the main drawbacks of this approach is that the amount of drug that can be loaded is very low due to the external layer, which must be very thin to avoid affecting the overall magnetic properties of the device. On the other hand, only one type of drug molecule can be loaded (hydrophilic or hydrophobic), and so their use as co-delivery systems is impossible. Indeed, many different diseases present a strong need to assess the co-delivery of multiple drugs to enable multitherapy that can work simultaneously against different biochemical pathways.[29,30] As an example, recent knowledge on diseases of the central nervous system shows that devices capable of simultaneously releasing drugs to different cell phenotypes, such as microglia, astrocytes, and neurons, can help to improve medical outcomes.[31–33] With respect to cancer therapy, it has also been demonstrated that multitherapy is better than monotherapy in terms of efficacy and safety.[34,35] We recently developed a tunable library of bijel-like structures, biphasic porous structures capable of loading and

E. Lacroce, F. Pizzetti, N. M. B. Urrego, G. Nunziata, M. Masi, F. Rossi
Department of Chemistry
Materials and Chemical Engineering 'Giulio Natta'
Politecnico di Milano
Piazza Leonardo da Vinci 32, Milan 20133, Italy
E-mail: filippo.rossi@polimi.it

The ORCID identification number(s) for the author(s) of this article can be found under https://doi.org/10.1002/mabi.202400084

DOI: 10.1002/mabi.202400084

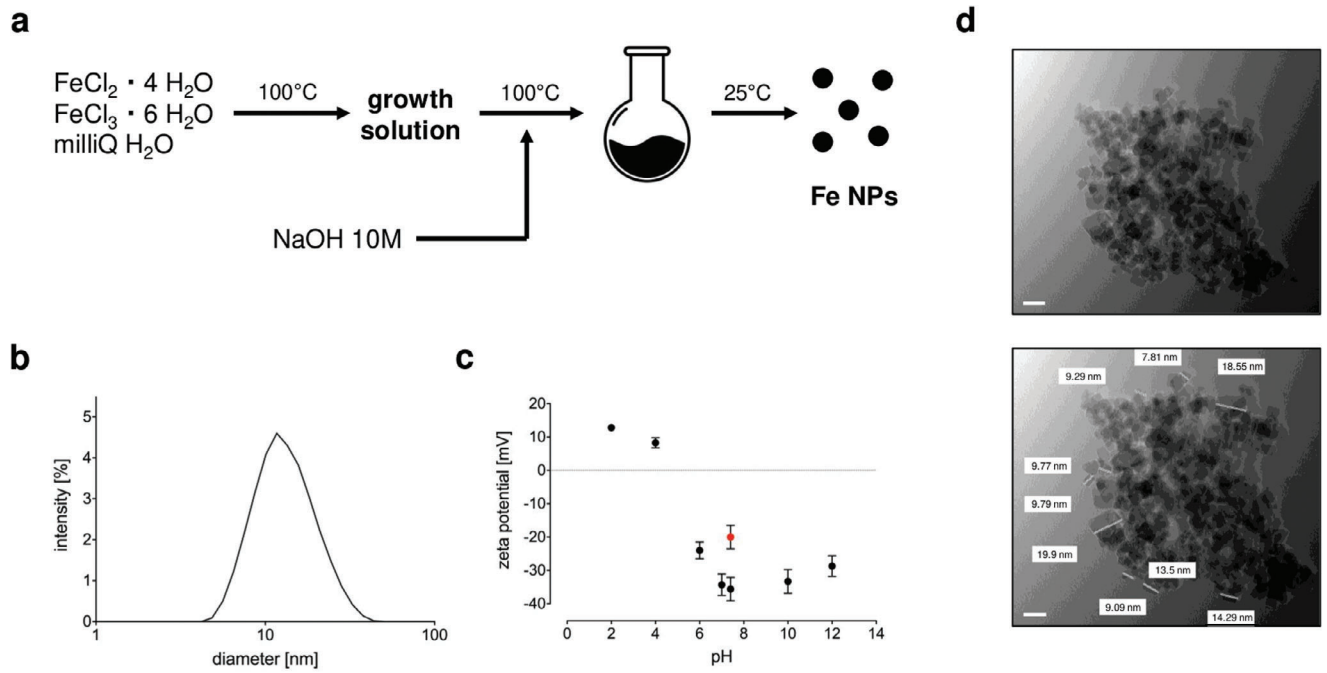

Figure 1. a) Schematic illustration of the synthetic route used to produce Fe NPs; b) size analysis of Fe_3O_4 NPs using DLS; c) zeta potential of Fe_3O_4 NPs in water (black circles) and in PBS (red circle) using DLS; d) TEM images of Fe_3O_4 NPs (scale bar = 20 nm).

simultaneously releasing hydrophilic and hydrophobic molecules.[36,37] These are bicontinuous structures where hydrophobic polymer (oil) and water are present in similar amounts and the final structure is retained and stabilized by the presence of nanoparticles (NP) at the interface without using surfactants.[38,39] In particular we propose the use of ϵ-caprolactone (CL) as the oil phase, which, together with a biocompatible initiator (ethanol) and catalyst (triazabicyclodecene, TBD) undergoes ring-opening polymerization, forming a polymer that is hydrophobic as well. Then, at the proper time before complete polymerization, iron oxide NP dispersion was added with the consequent formation of a three-dimensional structure. Here we study the formation of similar structures using iron oxide nanoparticles that can add to the magnetic properties of the system, making them promising tools for magnetically driven drug delivery.

2. Results and Discussion

2.1. Preparation and Characterization of Fe_3O_4 NPs

The basic steps necessary to produce iron-based NPs are presented in **Figure** 1a. Production started with a growth solution, NaOH was added, and finally recovered using an external magnet as described in detail in the Experimental Section. The resulting NPs were characterized in terms of X-ray diffraction (XRD) dimension, superficial charge, shape, and stability. The synthesized NPs showed peaks at 2θ values of 18.27°, 30.13°, 35.44°, 43.21°, 53.44°, 56.90°, and 62.65° related to the iron oxide (Fe_3O_4) pattern. The crystal phase of Fe_3O_4 NPs matched with that of magnetite demonstrating a good crystallinity (Figure S1, Supporting Information).[41] Dynamic light scattering (DLS) analysis showed a mean dimension of about 15 nm (Figure 1b). Moreover, the dependence of superficial charge on pH was studied in water and a buffered solution (PBS, red circle). The trend in water showed positive values at an acidic pH while negative charges were found for pH values higher than 4 (Figure 1d). The value obtained in the presence of PBS, which is typical of biomedical applications, is ≈−20 mV (red circle in Figure 1c), in accordance with previous studies.[42] The difference between the value obtained in water and in PBS at the same pH results from the presence of electrolytes in PBS that partially screen the charges, reducing the overall value. The dimension obtained from DLS analysis was also confirmed by transmission electron microscopy (TEM) analysis that also showed the cubic shape of Fe_3O_4 NPs in accordance with previous works (Figure 1d).[43,44]

2.2. Preparation and Characterization of Biphasic Porous Structures

The preparation of the iron-based biphasic structure starts with the polymerization of ϵ-caprolactone, a hydrophobic monomer that in bulk and in the presence of a catalyst and initiator represents the oil phase of this particular Pickering emulsion. Because bijels form a specific category of Pickering emulsions, the stability of the final system is possible thanks to the presence of nanoparticles present at the interface between the two immiscible phases, obviating the need for surfactants. In previous studies, we optimized the procedure using hydroxyapatite NPs and polyethylene glycol-polyethyleneimine NPs while here we investigate the possibility of using Fe_3O_4 NPs in the formation of these systems.[36,45] **Figure** 2a shows a schematic representation of the steps necessary to produce iron-based bijels. A syringe is used

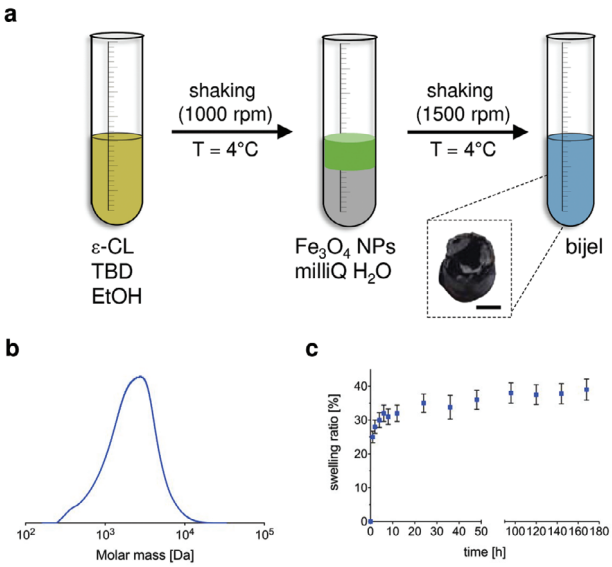

Figure 2. a) Schematic representation of the steps used for biphasic porous structures production and the photo of the bijel obtained (insert); b) GPC analysis of PCL in biphasic porous structures (blue line); c) swelling ratio of a biphasic porous structures in PBS (pH 7.4).

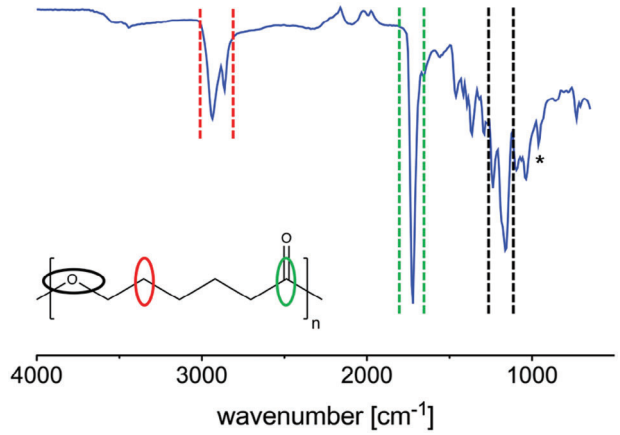

Figure 3. FTIR spectrum of iron-based bijel structures. The peaks at 2950 and 2860 cm^{-1} correspond to C-H groups (red), 1730 cm^{-1} to carbonyl groups (green), 1240 and 1150 cm^{-1} to C-O-C groups (black) of PCL. The peak at 953 cm^{-1} corresponds to the Fe-O bond (*).

to introduce ϵ-caprolactone, which starts to polymerize at room temperature in bulk conditions. The syringe was mixed using a shaker (details in Experimental Section) for an optimized amount of time before an aqueous dispersion of Fe_3O_4 NPs was dropped into the system, leading to the formation of a biphasic structure. This optimization is necessary to obtain a final solid structure and not a phase-separated liquid system. Indeed, the early addition of the aqueous dispersion of NPs inhibits polymerization while late addition does not guarantee interpenetration of the two phases. Both situations lead to phase separation between the oil and aqueous phases.

At the end of the procedure, the biphasic system is removed from the syringe without water loss as visible in Figure 2a insert and Figure S2 (Supporting Information). All the samples showed high stability at 37 °C without breakage (data not shown). This temperature is typical of biological tissues, making these devices desirable for biomedical applications.[46,47] The resulting polymer was then dissolved in tetrahydrofuran (THF) and analyzed with gel permeation chromatography (GPC) (Figure 2b) to understand the impact of Fe_3O_4 NPs on the polymerization of ϵ-caprolactone. Similar to other studies, we see that the presence of NPs only partially affects the formation of the polymer.[36] Indeed the number-averaged molecular weight is ≈1600 g mol^{-1}, the weight-averaged molecular weight is ≈2600 g mol^{-1} and the polydispersity index is 1.62. In contrast with hydrophobic matrices, the final bijel shows an ability to retain water without dissolving. This property is typical of hydrogels, hydrophilic networks known as swelling behavior, which can be seen in Figure 2c. The bijel samples showed superabsorbent characteristics with a swelling equilibrium reached after 8 hours with a 35% increase in term of weight. Another important characteristic is biocompatibility, which was assessed by culturing fibroblasts in vitro followed by an MTS assay. This test is commonly used as a test for the biocompatibility of biomaterials and the results showed no differences between cells in contact with bijels (BIJEL in Figure S3, Supporting Information) and without contact (CTRL in Figure S3, Supporting Information). From the Fourier tranformed infrared (FTIR) bijel spectrum, typical signals of Fe_3O_4 NPs and polycaprolactone are visible in **Figure 3**. Polycaprolactone peaks can be seen at 2950 and 2860 cm^{-1}, corresponding to C—H asymmetric and symmetric stretching of hydroxyl groups (red circles). Moreover, the peak at 1730 cm^{-1} is also related to polycaprolactone, in particular the carbonyl stretch vibration of esters (grey circle). In addition, C-O-C groups (black circle) are clearly visible at 1240 cm^{-1} (asymmetric stretching) and 1150 cm^{-1} (symmetric stretching) in accordance with previous works.[48,49] Fe_3O_4 NPs correspond to the peak at 953 cm^{-1} (Fe-O bond, * in Figure 3) that underline their presence within the biphasic structure.[50]

In previous studies, we checked for the presence of the two continuous phases using nuclear magnetic resonance (NMR) DOSY experiments, but this was not possible in this case due to the presence of magnetic NPs, which enables the use of NMR.[36,51] The biphasic structure was verified using environmental scanning electron microscopy (ESEM) analysis (Figures 4 and S4) on lyophilized samples (Figure 4a,b). Figure 4c shows carbon EDS, corresponding to the polyester phase, while the iron EDS map in Figure 4d is related to the presence of Fe_3O_4 NPs. It is clear that polycaprolactone is in the bulk phase while NPs are present at the interface. The corresponding EDS spectra confirming this interpretation are visible in Figure S5 (Supporting Information). The porosity of the final system is also observable using pyrene, a fluorescent tracer soluble only in hydrophobic phase (Figure S5, Supporting Information). The two different phases are well observable in Figure S5c,d: in both these images the black holes (not colored due to the incompatibility with pyrene) represents the water phase.

2.3. Magnetization of Biphasic Porous Structures

The magnetization curves were obtained at room temperature for Fe_3O_4 NPs (black line) and iron-based bijels (blue line) with applied magnetic fields of up to 2T (**Figure 5**a). All the samples

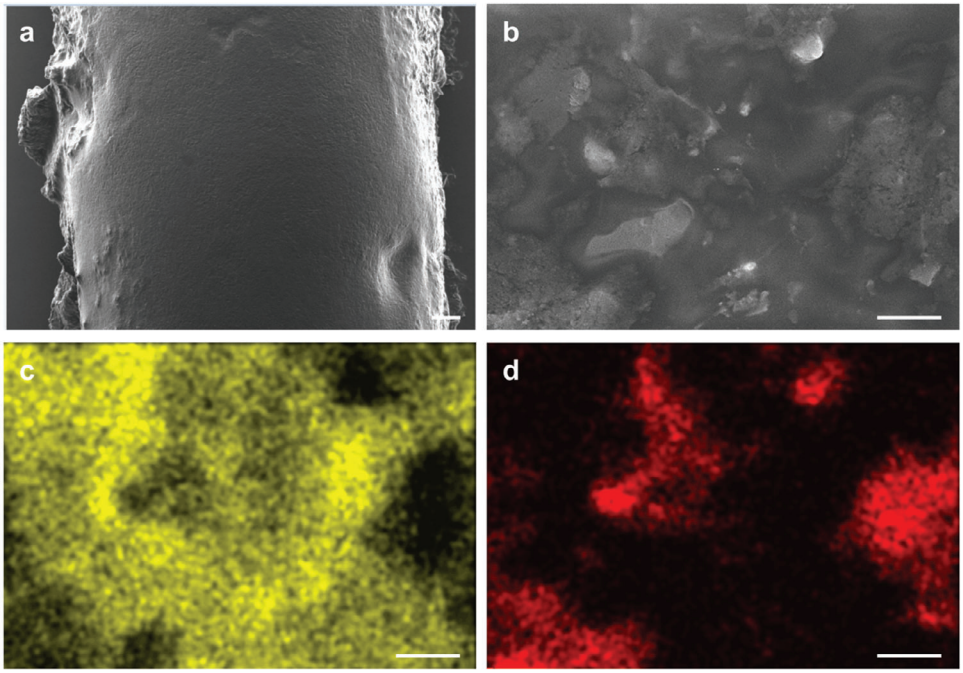

Figure 4. a, b) SEM analysis of biphasic porous structure; c) EDS image on C presence within the sample; d) EDS image on Fe presence within the sample. Scale bars: 100 μm (a); 20 μm (b–d).

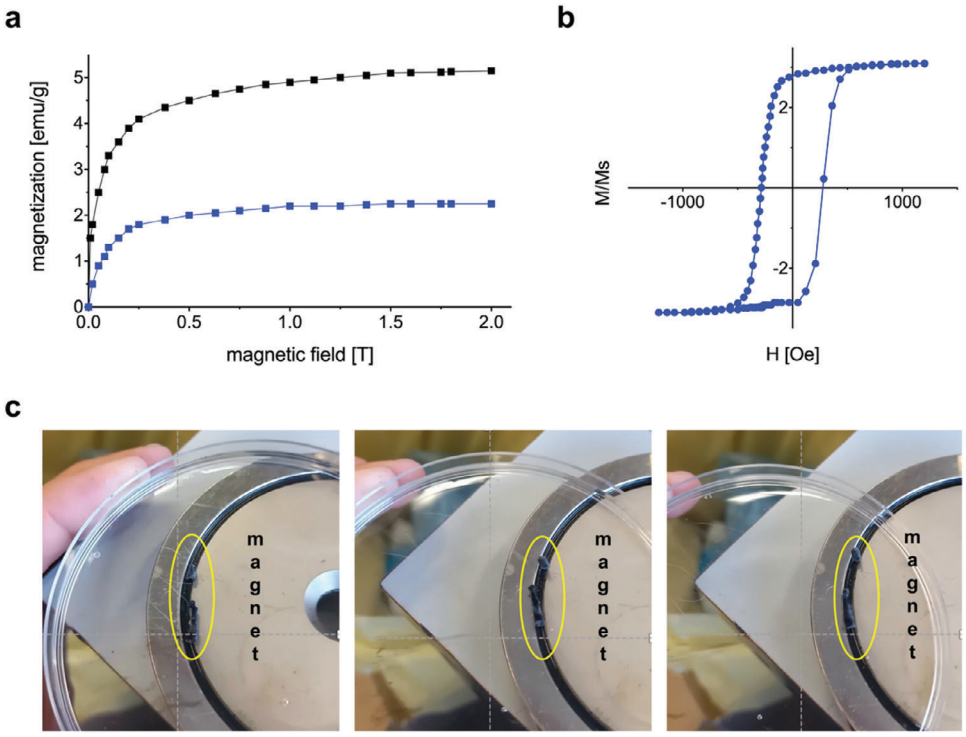

Figure 5. a) Magnetization of biphasic porous structure (blue line) vs iron oxide NPs (black line); b) magnetic hysteresis loop for the obtained biphasic porous structure; c) images of the iron-based bijels (yellow circle) attracted by the magnet.

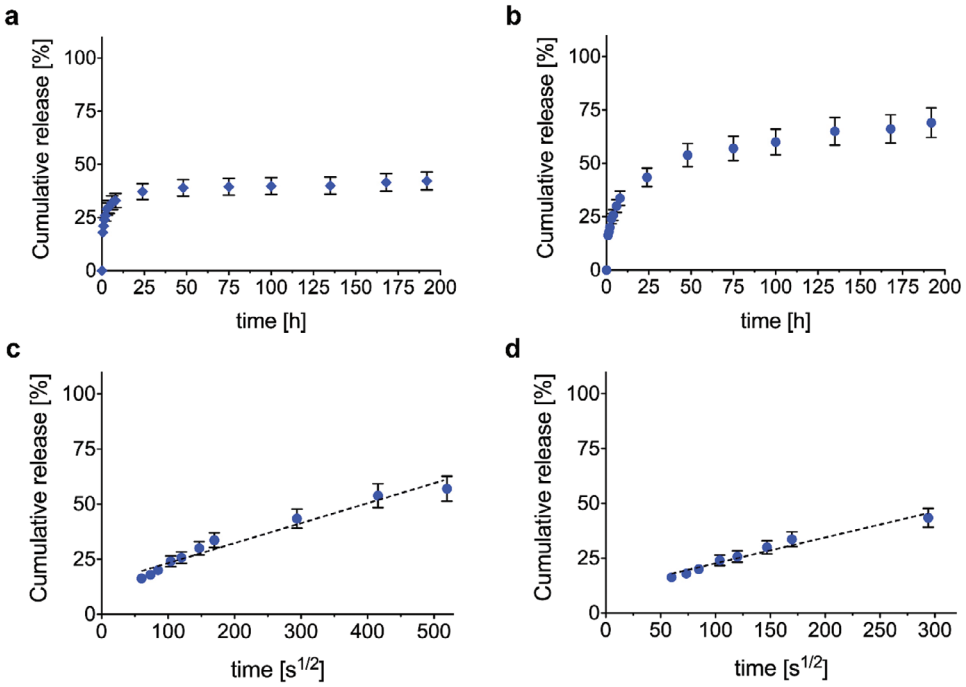

Figure 6. a) In vitro release profile of FITC delivered from a biphasic porous structure; b) in-vitro release profile of SF delivered from a biphasic porous structure; c,d) the slope of drug release against the square root of time represents Fickian diffusion coefficients for each sample ($p < 0.001$ between all groups). The cumulative release (%) is calculated relative to the amount of drug loaded ($n = 3$, mean ± standard deviation).

tested were almost saturated in this field, underling the absence of remanence with the experimental set-up. The bijel samples exhibited magnetic saturation two times lower than neat NPs due to the presence of polycaprolactone and water. Their presence only partially influences the magnetic properties of the entire device, as shown in previous studies.[26,52] The magnetic tests performed confirmed the superparamagnetic property of both Fe_3O_4 NPs and iron-based bijels, since the hysteresis loop is very limited (Figure 5b). This is as expected, given the small size of the NPs; indeed, it is well known that the critical size of magnetic NPs for showing these characteristics is ≈50 nm.[53] Figure 5c shows the magnetic properties of the final device attracted by the presence a magnet (details in Video S1, Supporting Information).

2.4. In Vitro Drug Delivery

The main advantage of these systems is that they can load and release drugs with different steric hindrance and water affinity simultaneously. For this investigation, we used three categories of commonly used drug mimetics to represent the conditions of low molecular weight hydrophobic drugs, low molecular weight hydrophilic drugs, and high molecular weight hydrophilic drugs.[54,55] Low molecular weight drugs (hydrophilic and hydrophobic) have a low steric hindrance and are commonly used as anti-inflammatory drugs, while high molecular weight drugs mimic biomolecules and antibodies used in several therapies.[56] The loading procedure, which ensures 100% loading efficiency, depends on the nature of the drug being loaded. In particular, hydrophilic drugs (here sodium fluorescein SF and fluorescein isothiocynate dextran FITC-DXT) are added in the second step (Figure 2a) and dissolved in water together with NPs, while hydrophobic compounds (here FITC) can be added in the monomer phase in the first step (Figure 2a). Samples were then placed in a Petri dish at 37°C in PBS and the release buffer was replaced at multiple times points. The data are represented as a percentage of the cumulative release of drugs loaded within the system (calibration lines in Figure S6, Supporting Information). **Figure 6** presents the release profiles of low steric hindrance drug mimetics: FITC (Figure 6a,c) and SF (Figure 6b,d). The release of FITC and SF are prolonged for more than 10 days with differences related to their water affinity. Along these lines, it can be seen that hydrophilic molecules have quicker rates considering the higher affinity with the aqueous environment. The drug mimetics showed sustained delivery without burst release, the uncontrolled contribution that represents drug molecule waste and thus the main drawback of controlled drug delivery systems. Burst release is typical of many hydrophilic devices such as hydrogels,[57,58] while the bijels developed in this study eliminate this unwanted effect for both hydrophobic and hydrophilic molecules. The release is therefore diffusion-driven starting from time 0; this can be seen by plotting release rates against the square root of time ($t^{1/2}$ in Figure 6c,d), where a linear correlation represents Fickian diffusion.[59] The slopes, which represent the diffusivity of the cargo through the carrier, show a difference between FITC and SF.

In particular, the SF slope is higher, with a clear linear region in the first 12 h, while FITC shows a flatter slope for more than 3 days. As expected from the literature on drug delivery, hydrophobic molecules are released with slower kinetics because this phenomenon is limited by water solubility. In addition, with bijels, we can not only sustain the release of low steric hindrance

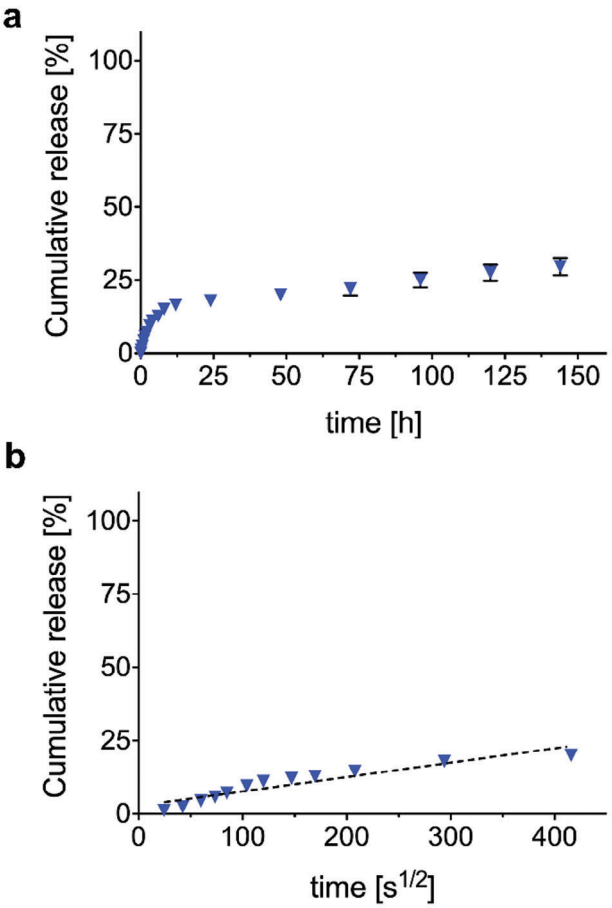

Figure 7. a) In vitro release profile of FITC-DXT 70 kDa delivered from a biphasic porous structure; b) the slope of drug release against the square root of time represents the Fickian diffusion coefficient for each sample ($p < 0.001$ between all groups). The cumulative release (%) is calculated relative to the amount of drug loaded ($n = 3$, mean ± standard deviation).

hydrophobic drugs, but also the release of hydrophilic drugs. We can also notice that the use of iron oxide NPs, respect to bijels already studied,[36,37] increases the release rates of both FITC and SF on one side but decreases the duration of pure Fickian diffusion and increases the percentage of uncontrolled release (burst release) on the other. This is probably a consequence of a higher swelling ability of bijels with iron oxide NPs (≈40%) in comparison with bijels without (≈30%) and consequent bigger pores.

Figure 7 presents the release of high steric hindrance hydrophilic molecules from bijels. In this case as well, the burst release is absent and the release is sustained for more than 10 days. As expected, the linear trend shows long-range Fickian diffusion behavior, underlining the suitability of these systems for proper delivery of high steric hindrance molecules such as antibodies and biomolecules.

3. Conclusion

The experiments discussed above demonstrated the possibility of preparing a magnetic device capable of carrying and releasing multiple drugs at the same time. In particular, this is made possible using paramagnetic nanoparticles that can be placed at the oil-water interface, stabilizing the system without being released. This procedure relies on a hydrophobic monomer that polymerizes under bulk conditions and, after being mixed with an NP aqueous colloid dispersion at the same volume, creates a three-dimensional structure that can maintain both phases without phase separation, partitioning them with NPs at the interface and obviating the use of surfactants. The resulting biphasic structure showed abilities typical of hydrophilic matrices (i.e., hydrogels) such as biocompatibility and swelling. It also solves classic drawbacks such as the difficulty in sustaining the release of hydrophilic drugs and the high correlated burst release. Given these results, magnetic bijels may be potential candidates for targeted delivery of drugs and biomolecules in medical applications.

4. Experimental Section

Materials: For biphasic porous structure synthesis, ϵ-caprolactone (CL), ethanol, and 1,5,7-triazabicyclo[4.4.0]dec-5-ene (TBD) were purchased from Merck (Deisenhofen, Germany). For the iron oxide nanoparticles, iron (II) chloride tetrahydrate ($FeCl_2 \cdot 4H_2O$, 98%), iron (III) chloride hexahydrate ($FeCl_3 \cdot 6H_2O$, 97%), and NaOH were purchased from Merck (previously Sigma–Aldrich Chemie GmbH, Deisenhofen, Germany). The fluorophores used as fluorescent drug mimetics in release tests included fluorescein sodium salt (SF), fluorescein isothiocyanate (FITC), and fluorescein isothiocyanate-dextran (FITC-DXT, MW = 70 kDa), produced by Merck (Germany). Products containing fluorescent molecules were stored in the dark at 4 °C until their use. All aqueous solutions were prepared using *milliQ* water. All reactants and solvents were used as received, without further purification. The solvents were of analytical grade. The reactions were carried out at atmospheric pressure.

Synthesis of Fe_3O_4 NPs: The co-precipitation method was used to synthesize the Fe NPs. First, 1.057 g of $FeCl_2 \cdot 4H_2O$ and 2.523 g of $FeCl_3 \cdot 6H_2O$ were dissolved in 106.6 mL of deionized water and the solution was stirred at 400 rpm at 100 °C for 1 h in a nitrogen atmosphere. Then, 33.3 mL of NaOH (10 M) was added to the reaction mixture, which was stirred for 1 h. Finally, the solution was cooled at room temperature and washed three times with distilled water. The NPs were recovered at the bottom of the flask after every wash using an external magnet (neodymium fishing magnet model NJD90 made by Wukong).

XRD Analysis: An X-ray diffraction experiment was carried out by SAMM laboratory at the Politecnico di Milano using the Empyrean diffractometer by Malvern Panalytical, equipped with Cu radiation (K-Alpha1, wavelength = 1.54060 Å). The experiment was performed at 25 °C.

Dynamic Light Scattering (DLS): DLS measurements were made using a Malvern Zetasizer Nano ZS at a scattering angle of 173° (backscatter). The temperature was kept at 25 °C and an equilibration time of 60 s was included before each measurement.

Transmission Electron Microscopy Analysis (TEM): Transmission electron micrographs were collected using a TEM-Zeiss LIBRA 200FE equipped with 200 kV FEG, in-column second-generation omega filter for energy selective spectroscopy (EELS) and imaging (ESI), HAADF STEM facility, EDS probe for chemical analysis and integrated tomographic HW and SW systems. TEM specimens were prepared by dropping an aqueous solution of NPs onto a carbon-coated copper grid (300 mesh) and evaporating the solvent. The particle size distribution was estimated using the ITEM-TEM Imaging platform by Olympus Soft Imaging Solutions.

Biphasic Porous Structure Synthesis: A mixture of CL (1 mL, 9.44 mmol, 1 eq.) was fed with ethanol (0.11 mL, 1.89 mmol, 0.2 eq.) as an initiator and TBD (26.5 mg, 0.189 mmol, 0.02 eq.) as a catalyst. The solution was mixed using a Heidolph Multi Reax shaker equipped with a 12-rack carousel at 1000 rpm for 8 minutes, according to the sample.

The same volume of iron oxide NP (20 mg mL^{-1}) colloidal dispersion in water was then introduced, and the shaking speed was increased to 1700

rpm for 40 s and then lowered to 1000 rpm for 5 min until the complete biphasic porous structure formed.

Fourier-Transform Infrared Spectroscopy (FTIR): FTIR transmission spectra were recorded using a Thermo Nexus 6700 spectrometer coupled to a Thermo Nicolet Continuum microscope equipped with a 15× Reflachromat Cassegrain objective at a resolution of 4 cm^{-1} using the ATR technique.

Gel Permeation Chromatography (GPC): GPC analyses were carried out using a Jasco LC-2000Plus gel permeation chromatograph coupled with a refractive index detector (RI-2031Plus, Jasco) using 3 Agilent PLgel columns, 5×10^6 M particle size, 300 × 7.5 mm (MW range: 5×10^2 to 17×10^5 g mol^{-1}). The GPC samples were injected using a Jasco AS-2055Plus autosampler. The instrument was calibrated using polystyrene standards. The analyses were carried out using THF as an eluent with a 0.5 mL min^{-1} flow rate at a temperature of 25 °C.

Swelling Behavior: Biphasic porous structures were lyophilized immediately after the synthesis and weighed (w_0). The samples were then immersed in PBS, stored at 37 °C, and removed at certain times to be weighed again (w_t). The collection times were initially more frequent for monitoring any eventual fast swelling kinetics. The mass swelling ratio was evaluated using Equation (1):

$$\textit{swelling ratio}\ [\%] = \frac{w_t - w_0}{w_0} \cdot 100 \quad (1)$$

Drug Loading: Due to their double nature, biphasic porous structures can entrap both hydrophilic and hydrophobic molecules. The cargo loading procedure is different if the molecules are hydrophilic or hydrophobic. The former can be dissolved directly in the aqueous solution of NPs, whereas the latter should be added to the ϵ-caprolactone prior to polymerization. As described in paragraph 2.6 we used 1 mL of ϵ-caprolactone and 1 mL of Fe_3O_4 NPs aqueous dispersion (20 mg mL^{-1}). The concentration of the drug mimetic used here was 0.05 mg mL^{-1} for FITC (solved in e-caprolactone), 0.1 mg mL^{-1} for SF (solved in water), and 1 mg mL^{-1} for FITC-DXT (solved in water).

Drug release Experiments: Release assays involved fluorescent tracers released from the scaffold, relying on the relation between concentration and absorbance described by the Lambert–Beer equation.[40] Absorbance was measured using the Tecan Microplate Reader spectrophotometer at the highest excitation wavelength typical of each tracer (SF = 485 nm, FITC and FITC-DXT = 500 nm). The cargo was loaded during the biphasic porous structure synthesis, and different types of fluorescent molecules were tested. After drug loading each bijel was immersed in excess of PBS solution (3 mL at pH 7.4) in a 12-well plate and release kinetics was monitored during time at 37 °C and 5% CO_2, resembling human body conditions. At each time point all PBS was removed, analyzed with UV, and replaced with fresh one. The amount of fluorophore released (cumulative release) was evaluated using Equation (2):

$$\textit{Cumulative release}\ [\%] = \frac{m^t_{tot}}{m_0} \cdot 100 \quad (2)$$

where m^t_{tot} is the overall drug released at time t and m_0 is the initial drug mass.

Scanning Electron Microscopy Analysis (SEM): SEM analysis was performed on gold sputtered samples at 10 kV with Evo 50 EP Instrumentation (Zeiss, Jena, Germany). To preserve the actual morphology of the biphasic porous structures, the samples were freeze-dried (for 24 h) to remove all the liquid by sublimation. Because of the low operating temperature and pressure, the polymer chains were expected to retain the same conformation they had under wet conditions. Comparative evaluation of the surface and internal morphology of the samples was performed.

Fluorescent Confocal Microscopy: Fluorescent confocal microscopy analyses have been performed introducing a fluorescent tracer inside the biphasic porous structures: pyrene that is soluble in the hydrophobic phase. Images were collected using an Olympus Fv1000 confocal microscope (Laser 594 nm).

Cytotoxicity: Mouse fibroblasts (L929) were cultured in complete medium (Dulbecco's modified Eagle's medium (DMEM) supplemented with 10% fetal bovine serum, 1% penicillin/streptomycin, 1% L-glutamine 200 mM). Cells were maintained at 37 °C in 5% CO_2. Three-dimensional macrostructures formed and were placed in cell culture inserts. L929 were seeded in 24-well plates at a concentration of 50 000 cells/well in 1 mL of complete medium and grown at 37°C, 5% CO_2. After 24 h, the medium was changed and the inserts with biphasic porous structures were added in contact with the medium. After 3 days of culturing, the cytotoxicity of the macrostructure was evaluated by performing an MTS assay. The absorbance was measured at 570 nm, and the results were compared with the results of the control wells to determine relative cell viability.

Statistical Analysis: Experimental data were analyzed using analysis of variance (ANOVA). Statistical significance was set to a p-value < 0.05. The results are presented as a mean value ± standard deviation.

Supporting Information

Supporting Information is available from the Wiley Online Library or from the author.

Conflict of Interest

The authors declare no conflict of interest.

Author Contributions

E.L. and F.P. contributed equally to this work. E.L. and F.P. performed methodology, validation, and wrote the original draft. Nicola M. Barbosa Urrego: Methodology, Validation. G.N. performed methodology and validation. M.M. conceptualization, and reviewed and edited the final manuscript. F.R. performed conceptualization, supervision, and reviewed and edited the final manuscript.

Data Availability Statement

The data that support the findings of this study are available from the corresponding author upon reasonable request.

Keywords

bijels, colloids, drug delivery, iron nanoparticles, polymers

Received: February 26, 2024
Revised: April 23, 2024
Published online:

[1] B. Wang, L. Hu, T. J. Siahaan, *"Drug Delivery: Principles and Applications"*, John Wiley& Sons, New York **2016**.
[2] J. Gao, J. M. Karp, R. Langer, N. Joshi, *Chem. Mater.* **2023**, *35*, 359.
[3] M. Rowland, *J. Pharm. Sci.* **1972**, *61*, 70.
[4] O. C. Farokhzad, R. Langer, *Adv. Drug Delivery Rev.* **2006**, *58*, 1456.
[5] J. H. Lee, Y. Yeo, *Chem. Eng. Sci.* **2015**, *125*, 75.
[6] K. Park, *J. Controlled Release* **2014**, *190*, 3.
[7] M. Ishak Khan, M. Imran Hossain, M. Khalid Hossain, M. H. K. Rubel, K. M. Hossain, A. M. U. B. Mahfuz, M. I. Anik, *ACS Appl. Bio Mater.* **2022**, *5*, 971.
[8] Y. Liu, Q. Li, Q. Bai, W. Jiang, *J. Mater. Chem. B* **2021**, *9*, 5439.

[9] P. Liu, G. Chen, J. Zhang, *Molecules* **2022**, *27*, 1372.
[10] M. Ghezzi, S. Pescina, C. Padula, P. Santi, E. Del Favero, L. Cantù, S. Nicoli, *J. Controlled Release* **2021**, *332*, 312.
[11] M. J. Mitchell, M. M. Billingsley, R. M. Haley, M. E. Wechsler, N. A. Peppas, R. Langer, *Nat. Rev. Drug Discovery* **2020**, *20*, 101.
[12] H. J. K. Mohit, J. Mehta, S. B. Lim, Mitsuru Naito, Kanjiro Miyata, *Macromol. Biosci.* **2024**, 2300366.
[13] M. Awashra, P. Mlynarz, *Nanoscale Adv* **2023**, *5*, 2674.
[14] Y. Ju-Nam, J. R. Lead, *Sci. Total Environ.* **2008**, *400*, 396.
[15] C. M. Oral, M. Pumera, *Nanoscale* **2023**, *15*, 8491.
[16] P. L. Venugopalan, B. Esteban-Fernández de Ávila, M. Pal, A. Ghosh, J. Wang, *Fantastic Voyage of Nanomotors into the Cell* **2020**, *14*, 9423.
[17] D. R. Yao, I. Kim, S. Yin, W. Gao, *Adv. Mater.* **2024**, *36*, 2308829.
[18] T. Xu, J. Yu, X. Yan, H. Choi, L. Zhang, *Micromachines* **2015**, *6*, 1346.
[19] F. Cheng, R. Yin, Y. Zhang, C. C. Yen, Y. Yu, *Soft Matter* **2010**, *6*, 3447.
[20] S. Takatsuka, T. Kubota, Y. Kurashina, H. Onoe, *Small* **2023**, *19*, 2204139.
[21] R. Bernasconi, E. Mauri, A. Rossetti, S. Rimondo, R. Suriano, M. Levi, A. Sacchetti, S. Pane, L. Magagnin, F. Rossi, *Mater. Des.* **2021**, *197*, 109212.
[22] B. J. Nelson, S. Pane, *Science* **2023**, *382*, 1120.
[23] H. Shen, S. Cai, Z. Wang, Z. Ge, W. Yang, *Mater. Des.* **2023**, *227*, 111735.
[24] M. Koleoso, X. Feng, Y. Xue, Q. Li, T. Munshi, X. Chen, *Mater. Today Bio* **2020**, *8*, 100085.
[25] J. Llacer-Wintle, A. Rivas-Dapena, X. Z. Chen, E. Pellicer, B. J. Nelson, J. Puigmartí-Luis, S. Pane, *Adv. Mater.* **2021**, *33*, 2102049.
[26] R. Bernasconi, F. Cuneo, E. Carrara, G. Chatzipirpiridis, M. Hoop, X. Chen, B. J. Nelson, S. Pane, C. Credi, M. Levi, L. Magagnin, *Mater. Horiz.* **2018**, *5*, 699.
[27] Z. Xiang, G. Jiang, D. Fan, J. Tian, Z. Hu, Q. Fang, *Nanoscale* **2020**, *12*, 13513.
[28] U. Bozuyuk, O. Yasa, I. C. Yasa, H. Ceylan, S. Kikilel, M. Sitti, *ACS Nano* **2018**, *12*, 9617.
[29] N. Li, L. Zhao, L. Qi, Z. Li, Y. Luan, *Prog. Polym. Sci.* **2016**, *58*, 1.
[30] H. Chun, M. Yeom, H. O. Kim, J. W. Lim, W. Na, G. Park, C. Park, A. Kang, D. Yun, J. Kim, D. Song, S. Haam, *Polym. Chem.* **2018**, *9*, 2116.
[31] I. Vismara, S. Papa, V. Veneruso, E. Mauri, A. Mariani, M. De Paola, R. Affatato, A. Rossetti, M. Sponchioni, D. Moscatelli, A. Sacchetti, F. Rossi, G. Forloni, P. Veglianese, *ACS Nano* **2020**, *14*, 360.
[32] Z. Giorgi, V. Veneruso, E. Petillo, P. Veglianese, G. Perale, F. Rossi, *ACS Appl. Bio Mater.* **2024**, *7*, 80.
[33] V. Veneruso, E. Petillo, F. Pizzetti, A. Orro, D. Comolli, M. De Paola, A. Verrillo, A. Baggiolini, S. Votano, F. Castiglione, M. Sponchioni, G. Forloni, F. Rossi, P. Veglianese, *Adv. Mater.* **2024**, *36*, 2307747.
[34] S. Fumoto, K. NIshida, *Chem. Pharm. Bull.* **2020**, *68*, 603.
[35] R. D. Al Bostami, W. H. Abuwatfa, G. A. Husseini, *Nanomaterials* **2022**, *12*, 2672.
[36] F. Pizzetti, A. Rossetti, A. Marchetti, F. Castiglione, V. Vanoli, E. Coste, V. Veneruso, P. Veglianese, A. Sacchetti, A. Cingolani, F. Rossi, *Adv. Mater. Interf.* **2021**, *8*, 2100991.
[37] F. Pizzetti, G. Massobrio, S. Riva, F. Briatico Vangosa, F. Rossi, *Gels* **2024**, *10*, 72.
[38] M. F. Haase, K. J. Stebe, D. Lee, *Adv. Mater.* **2015**, *27*, 7065.
[39] S. P. Kharal, R. P. Hesketh, M. F. Haase, *Adv. Funct. Mater.* **2020**, *30*, 2003555.
[40] H. S. Kim, J. H. Kang, J. H. Jang, E. J. Lee, J. H. Kim, J. Byun, U. S. Shin, *Eur. J. Pharm. Sci.* **2023**, *188*, 106525.
[41] A. Ali, M. S. AlSalhi, M. Atif, A. A. Ansari, M. Q. Israr, J. R. Sadaf, E. Ahmed, O. Nur, M. Willander, *J. Phys. Conf. Ser.* **2013**, *414*, 012024.
[42] C. Turrina, S. Berensmeier, S. P. Schwaminger, *Pharmaceuticals* **2021**, *14*, 405.
[43] A. Shavel, L. M. Liz-Marzan, *Phys. Chem. Chem. Phys.* **2009**, *11*, 3762.
[44] C. de Montferrand, L. Hu, I. Milosevic, V. Russier, D. Bonnin, L. Motte, A. Brioude, Y. Lalatonne, *Acta Biomater.* **2013**, *9*, 6150.
[45] V. Vanoli, G. Massobrio, F. Pizzetti, A. Mele, F. Rossi, F. Castiglione, *ACS Omega* **2022**, *7*, 42845.
[46] T. J. Thorson, R. E. Gurlin, E. L. Botvinivk, A. Mohraz, *Acta Biomater.* **2019**, *94*, 173.
[47] T. J. Thorson, E. L. Botvinivk, A. Mohraz, *ACS Biomater. Sci. Eng.* **2018**, *4*, 587.
[48] J. S. Lyu, J. S. Lee, J. Han, *Sci. Rep.* **2019**, *9*, 20236.
[49] A. Abdolmaleki, Z. Mohamadi, *Colloid Polym. Sci.* **2013**, *291*, 1999.
[50] A. El Nemr, M. A. Hassaan, M. R. Elkatorym, S. Ragab, A. Pantaleo, *Molecules* **2021**, *26*, 5105.
[51] A. Partenope, F. Pizzetti, V. Vanoli, M. Casalegno, A. Cingolani, L. Parreiras Nogueira, F. Castiglione, H. J. Haugen, F. Rossi, *Mater. Today Comm.* **2022**, *33*, 104290.
[52] A. Pardo, M. Gomez-Florit, S. Barbosa, P. Taboada, R. M. A. Domingues, M. E. Gomes, *ACS Nano* **2021**, *15*, 175.
[53] Y. Hadadian, H. Masoomi, A. Dinari, C. Ryu, S. Hwang, S. Kim, B. K. Cho, J. Y. Lee, J. Yoon, *ACS Omega* **2022**, *7*, 15996.
[54] J. Sakata, T. Tatsumi, A. Sugiyama, A. Shimizu, Y. Inagaki, H. Katoh, T. Yamashita, K. Takahashi, S. Aki, Y. Kaneko, T. Kawamura, M. Miura, M. Ishii, T. Osawa, T. Tanaka, S. Ishikawa, M. Tsukagoshi, M. Chansler, T. Kodama, M. Kanai, H. Tokuyama, K. Yamatsugu, *Protein Expr. Purif.* **2024**, *214*, 106375.
[55] T. Casalini, M. Salvalaglio, G. Perale, M. Masi, C. Cavallotti, *J. Phys. Chem. B* **2011**, *115*, 12896.
[56] S. Koutsopoulos, L. D. Unsworth, Y. Nagai, S. Zhang, *Proc. Natl. Acad. Sci. USA* **2009**, *106*, 4623.
[57] C. M. L. Lau, G. Jahanmir, Y. Yu, Y. Chau, *J. Controlled Release* **2021**, *335*, 75.
[58] X. Huang, C. S. Brazel, *J. Controlled Release* **2001**, *73*, 121.
[59] K. Vulic, M. S. Shoichet, *J. Am. Chem. Soc.* **2012**, *134*, 882.